

Metal oxide-assisted chemical synthesis of poly(α -naphthylamine) and characterizations

S. Radhika · K. Durai Murugan · I. Baskaran ·
V. Dhanalakshmi · R. Anbarasan

Received: 27 December 2008 / Accepted: 8 April 2009 / Published online: 29 April 2009
© Springer Science+Business Media, LLC 2009

Abstract α -Naphthylamine (NA) was chemically polymerized using peroxy disulfate (PDS) as a chemical initiator under inert atmosphere at 45 °C with vigorous stirring under various experimental conditions such as different concentrations of NA, PDS and different % weight of nanosized metal oxides like Sb_2O_3 , CrO_3 , V_2O_5 , Al_2O_3 , As_2O_3 and ammonium heptamolybdate (AHM). Chemical kinetics inferred that rate of polymerization (R_p) is 1.75 order of reaction with [NA] and 1.0 with [PDS]. FTIR spectroscopy confirmed that both benzenoid and quinonoid rings built up the structure of poly(α -naphthylamine) (PNA). Added metal oxides influenced the R_p , char forming capability of PNA and conductivity too through their surface catalytic effect. AFM confirmed the presence of nanosized materials in the polymer–nanocomposite structure. HRTEM was used to confirm the nanosize of metal oxides and the intercalation of PNA chains into the basal spacing of metal oxides.

Introduction

For the past few decades, the polymer chemists have turned their attention toward the chemical [1] and

electrochemical [2] synthesis of mononuclear aromatic primary and secondary amines due to their high conductivity, ease of preparation, environmental stability and their potential applications in different engineering and medical fields [3]. Unfortunately, publications on polynuclear aromatic amines are rarely available in the literature. Baghahi et al. [4] reported the electrochemical synthesis of poly(β -naphthylamine) in aqueous acidic medium. Electrochemical polymerization of α -naphthylamine (NA) in perchloric acid medium was reported in [5]. Electropolymerization of NA in the eutectic mixture has been reported in literature [6]. Ferrocene sulfonic acid-doped poly(α -naphthylamine) (PNA) was electrochemically prepared and characterized by using FTIR, XPS, SEM, and cyclic voltammetry [7]. Moon et al. [8] reported about chemical oxidative polymerization and characterization of PNA and poly(1-amino anthracene). Naphthylamines were electrochemically oxidized in aqueous acidic medium in the presence of KI [9]. Arevalo et al. [10] have studied the electropolymerization of NA in aqueous acidic medium and explained the mechanism of polymerization. Simultaneous UV–visible, spectroelectrochemical, and quartz crystal measurements of PNA film was published in the year 1995 [11]. Roy et al. [12] recently published chemical oxidative polymerization of NA and β -naphthylamine. In 2002, George and Young reported the self-doped water-soluble poly(naphthylamines) [13]. Gordana et al. [14] electropolymerized 2-methyl-1-naphthylamine and the films were characterized by using FTIR, CV and GPC techniques. Electrochemical polymerization of 5-amino naphthol [15], NA [16], and α -amino anthracene [17] has been reported in the literature. The above literature survey indicated the methods available for the synthesis of poly(naphthylamine) and analytical instruments used for their characterization.

S. Radhika · K. Durai Murugan · I. Baskaran
Department of Chemistry, S.N. College, Madurai 625 022,
Tamil Nadu, India

V. Dhanalakshmi
Department of Polymer Technology, KCET, Virudhunagar
626 001 Tamil Nadu, India

R. Anbarasan (✉)
Department of Chemical Engineering, Nano Biotechnology
Research Laboratory, National Taiwan University, Taipei 10617,
Taiwan, ROC
e-mail: anbu_may3@yahoo.co.in

Currently, FTIR spectroscopy plays a considerable role in research. Because of high sensitivity or detectivity toward trace amount of sample, low noise-to-signal ratio, FTIR spectrometer is used as a tool in various science and engineering fields. Moreover, this method is easy and inexpensive. FTIR spectroscopy is used for both qualitative [18–22] and quantitative [23–33] analysis. By taking the above-mentioned references as a model, we propose here a modified equation for the quantitative determination of percentage amino and imino forms in colored, rigid, and amorphous poly(naphthylamine). Our recent study proves that transmittance peak area is directly proportional to the concentration of the substance [33]. In this investigation for the first time, we report about the chemical synthesis of PNA–metal oxide nanocomposites and its characterization by various analytical techniques like FTIR, conductivity measurements, AFM, HRTEM, and TGA.

Experimental

Materials

α -Naphthylamine (NA, Merck, India), potassium salt of peroxy disulfate (PDS, AR, Merck), acetic acid (Ranbaxy, India), and sodium acetate buffer (SD Fine Chemicals, India) were purchased and used as received. Metal oxides like V_2O_5 (AR, Nice Chemicals, India), As_2O_3 (AR, Nice Chemicals), Al_2O_3 (AR, Nice Chemicals), Sb_2O_3 (AR, Nice Chemicals), ammonium hepta molybdate (AHM, Nice Chemicals, AR) and CrO_3 (SD Fine Chemicals) were purchased and used without further purifications. Doubly distilled (DD) water was used for solution preparation.

Synthesis of PNA and its nanocomposites

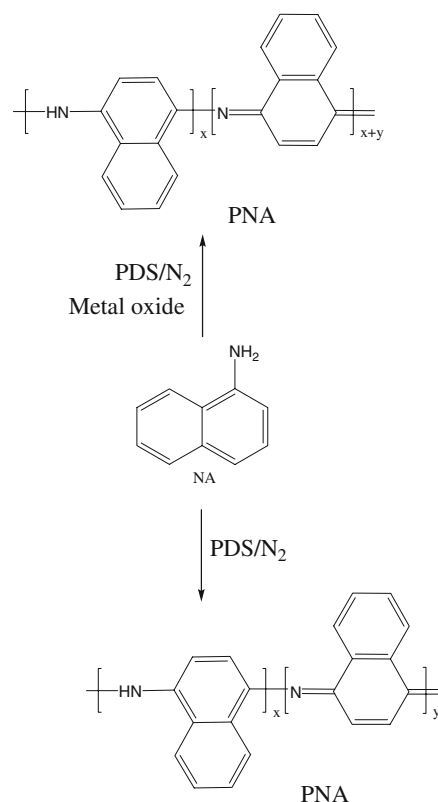
PNA was synthesized at different experimental conditions such as variation in concentration of monomer, initiator and for different interval of reaction time at different temperatures. In brief, α -NA (0.10 M) solution has been prepared by dissolving 1.4319 g of α -NA in acetic acid/sodium acetate buffer solution. The acidic buffer solutions (pH = 2.1) contain 0.05 M sodium acetate (25 mL) and 5 M of acetic acid (75 mL). 0.10 M PDS solution was prepared by dissolving 2.7303 g of PDS in 100 mL DD water. In brief, 20 mL of monomer has been taken in a polymerization reactor with nitrogen inlet and outlet. Pure nitrogen gas was purged through the solution for 30 min and the temperature of the system was maintained at 45 °C. Ten mL of initiator was added under vigorous stirring and purging was continued for the next 2 h. After 2 h of reaction time, the contents of dark green-colored precipitate was filtered by using previously weighed G4 sintered crucible (W_1 g) and dried at 80 °C for 6 h to remove the unbounded water molecules and buffer

solutions. The dried crucible with polymer was again weighed (W_2 g) and noted the difference in weight corresponding to the amount of polymer formed. From the amount of polymer formed, the rate of polymerization (R_p) was calculated by using the following formula:

$$\text{Rate of polymerization } (R_p) = \frac{\text{Weight of polymer}}{V \times t \times M} \times 1000, \quad (1)$$

where V is the volume of total reaction mixture, t is the reaction time (s) and M is the molecular weight of the monomer.

The same procedure was used for the preparation of polymer nanocomposites in the presence of metal oxides like Sb_2O_3 , CrO_3 , V_2O_5 , Al_2O_3 , As_2O_3 and AHM with required quantity. In brief, 20 mL of monomer solution was taken in a polymerization reactor under inert atmosphere at 45 °C. Ten mL of initiator and 5% weight of any one of the metal oxide were charged, and the time of addition of both initiator and metal oxide was taken as the starting of reaction time because some metal oxides are acting as an oxidizing agent, e.g., V_2O_5 , CrO_3 , etc. After 2 h of reaction time, the obtained green-colored precipitate was filtered through already weighed G4 sintered crucible. The difference in weight of empty crucible and crucible with polymer yielded the weight of the polymer obtained. The polymerization reaction is shown in Scheme 1.



Scheme 1 Chemical polymerization of NA in the presence and absence of metal oxide

Characterizations

FTIR spectrum is recorded for the polymer and its nanocomposites by using Shimadzu-8400 S model spectrophotometer through KBr pelletization method. TGA is recorded through NETZSCH Gretebau GmbH Thermal instrument at the heating rate of 10 °C/min under air atmosphere. Atomic force microscopy (AFM) for the samples is recorded by Olympus OMC (L-TR) 800-psa type instrument (2D) with the resonance frequency of 24 kHz. Conductivity value of the powder samples are determined by using Standard Four Probe conductivity meter (Model DFP-02). Furthermore, the topographical analysis of PNA nanocomposites are carried out by recording HRTEM using (TEM 3010) transmission electron microscopy (TEM) instrument, a product of JEOL.

Results and discussion

Recently, the polymer chemists are concentrating on the synthesis, characterizations and effective applications of polynuclear aromatic amines. Furthermore, the conductivity value of polyaromatic amines is influenced by changing the oxidative initiator, dopants and other experimental conditions. Currently, the electrical conductivity of polyaromatic amines has been improved by the addition of nanosized materials. In that series, we have tried to analyze the effect of nanosized material on the structure–property relationship of PNA via catalyzing the rate of polymerization (a simple kinetic study was carried out) and their corresponding conductivity and thermal stability values. The order of reaction can be determined by drawing a log-log plot (universally following method) and which can be further confirmed by drawing a direct plot. Due to simplicity, we have drawn only the most informative log-log plot. The effect of different experimental kinetic parameters on the order of reaction is discussed in the following sections.

FTIR spectroscopy

The FTIR spectrum of PNA is shown in Fig. 1a. Generally, the chemical structure of poly(aniline) (PANI) is made up of 50% amino nitrogen and 50% imino nitrogen. The chemical structure of PNA is also similar to that of PANI. While considering the FTIR spectrum of PNA, there are four important peaks. A broad peak around 3500 cm^{-1} is responsible for OH stretching of physisorbed water molecules. Peak at 720 cm^{-1} is due to C–H out of plane bending vibration. Peaks that appear at 1490 and 1590 cm^{-1} correspond to the amino and imino nitrogen of

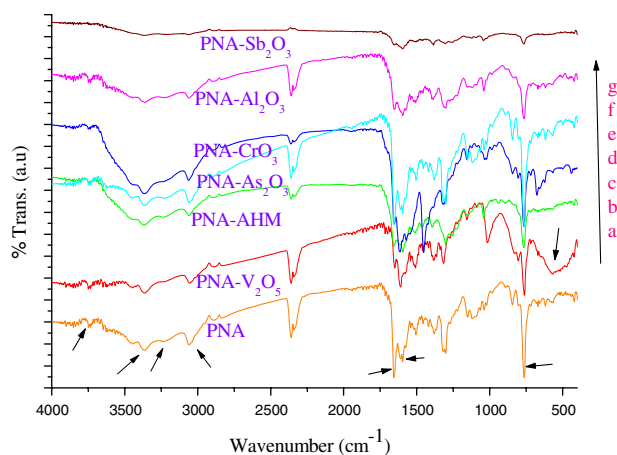


Fig. 1 FTIR spectrum of (a) PNA, (b) PNA- V_2O_5 , (c) PNA-AHM, (d) PNA- As_2O_3 , (e) PNA- CrO_3 , (f) PNA- Al_2O_3 , and (g) PNA- Sb_2O_3 . [NA] = 0.025 M, [PDS] = 0.025 M, time = 2 h, temperature = 45 °C, and nanomaterial = 5% weight

PNA, respectively. When a monomer interacts with an initiator radical, first, there will be a formation of anilinium radical cation (benzenoid structure) which on secondary oxidation yields imino nitrogen (quinoid structure). Chemical oxidation of NA also follows the same concept. A broad peak at 1031 cm^{-1} is due to the stretching of CH_3COO^- ion. A small peak at 1108 cm^{-1} is responsible for $\nu(\text{B-NH-Q})$, and the peak at 1301 cm^{-1} corresponds to $\nu(\text{C-N})$. Small peaks that appear between 400 and 1000 cm^{-1} is due to the M–O stretching of the metal oxides in the case of PNA nanocomposites. Figure 1b–g indicates the FTIR spectrum of PNA nanocomposites. Figure 2 represents the FTIR spectra of PNA nanocomposites. Recently, Anbarasan et al. [34] reported about the benzenoid to quinonoid ratio of PNA–clay nanocomposite system by using FTIR spectroscopy. Chang et al. [35] synthesized PANI/Au/MWCNT nanocomposite and characterized by using FTIR, XRD, XPS and TEM techniques. Our results coincide with their reports.

The basic concept in FTIR spectrum is the area of peak, which is directly proportional to the concentration of the material. In this study, we concentrate on three important peaks, namely benzenoid ring stretching (1490 cm^{-1}), quinonoid ring stretching (1590 cm^{-1}), and C–H out of plane bending vibration (720 cm^{-1}). Peak area is determined by using FTIR software after proper base line correction. Our recent publication proves that transmittance peak area is directly proportional to the concentration of the substance [33], i.e., the relative intensity (RI) of aliphatic ester is proportional to the amount of substance, which can be equalized by the introduction of proportionality constant. This can be written as

$$\text{RI}[A_{1745}/A_{1093}] \propto C \quad \text{and} \quad \text{RI}[A_{1745}/A_{1093}] = aC,$$

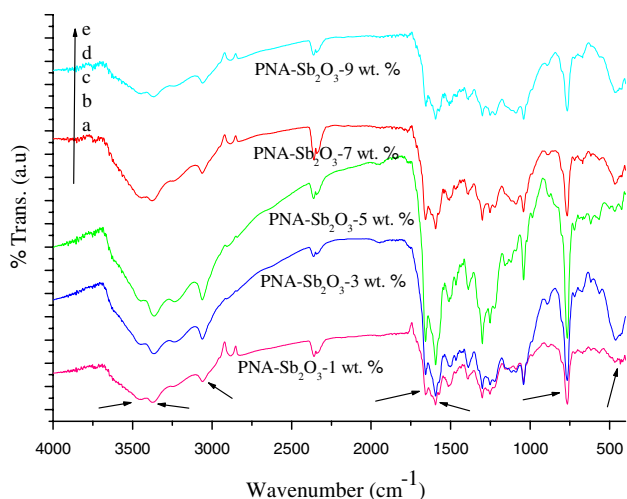


Fig. 2 FTIR spectrum of PNA with (a) 1% weight of Sb_2O_3 , (b) 3% weight of Sb_2O_3 , (c) 5% weight of Sb_2O_3 , (d) 7% weight of Sb_2O_3 , and (e) 9% weight of Sb_2O_3

where C is the concentration of the substance and a is a proportionality constant. This principle is applied for the present investigation and the values are reported.

We know that PANI backbone is made up of benzenoid, quinonoid, and semiquinonoid forms. The amount of formation of semiquinonoid form is negligible because it can be readily oxidized or reduced. Hence,

$$\text{Structure of PANI} = \% \text{amino form (benzenoid form)} + \% \text{imino form (quinonoid form)}$$

The concentration of amino form can be determined from the ratio of the relative intensity of benzenoid structure (appears in the FTIR spectrum at 1490 cm^{-1}) and C–H out of plane bending vibration (appears at 720 cm^{-1} , taken as an internal standard to nullify error).

$$RI[A_{1490}/A_{720}] \propto C \text{ and } RI[A_{1490}/A_{720}] = mC,$$

where m is a proportionality constant.

$$\text{Concentration of amino form} = X = RI[A_{1490}/A_{720}] \times W_1/W_2 \times 0.509.$$

$$\text{The concentration of imino form can be determined as } RI[A_{1590}/A_{720}] \propto C \text{ and } RI[A_{1590}/A_{720}] = nC$$

Concentration of imino form = $Y = RI[A_{1590}/A_{720}] \times W_1/W_2 \times 2.18$ where n is a proportionality constant. W_1 is the weight of polymer taken for FTIR study, W_2 is the weight of the initiator and 0.509 and 2.18 are the proportionality constants or calibration coefficients.

Currently, Anbarasan et al. [34] have published the results on the ratio of relative intensity of benzenoid and quinonoid forms, which predict the structure of PNA, structurally similar to PANI. In this study, we report the order of reaction based on the FTIR-based results for the first time.

Effect of time on R_p and the RI of benzenoid and quinonoid forms of PNA

R_p is calculated at different time intervals while other experimental conditions are kept constant. While plotting t vs. R_p (Fig. 3a), the graph shows a straight line with decreasing trend. This is due to the abnormal increase in time value (cf. Eq. 1).

While increasing the amount of time, the RI of both the benzenoid and quinonoid forms are increased linearly (Fig. 3b and c, respectively). This is due to: (1) Longer reaction time, which allows possible interaction among monomer radical cations. (2) Facilitating the coupling of oligomer radical cations. (3) Allowing both the possible primary and secondary oxidation reactions.

Effect of [NA] on R_p and the RI of benzenoid and quinonoid forms of PNA

[NA] is varied between 0.015 and 0.035 M while other experimental conditions are kept constant. While increasing the [NA], the R_p value is increased linearly. This can be ascribed to the availability of more number of monomer units available for the polymer chain growth. To find out the order of reaction, the plot of $\log R_p$ vs. $\log [NA]$ (Fig. 4a) is made and found as a straight line with a slope value of 1.75 with respect to [NA] and hence confirms the 1.75 order of reaction. This is due to the formation of more and more Naphthylamine radical cations and surface catalytic effect (auto acceleration effect) of formed PNA $\{R_p \propto [NA]^{1.75}\}$.

While increasing the concentration of NA, the relative intensity of benzenoid peak is increased. The increase in RI confirms the polymerization reaction. To find out the order of reaction corresponding to the benzenoid structure formation, the log-log plot is made. Figure 4b indicates the plot of $\log [NA]$ vs. $\log (RI_{[B/CH]})$. The plot gives a straight

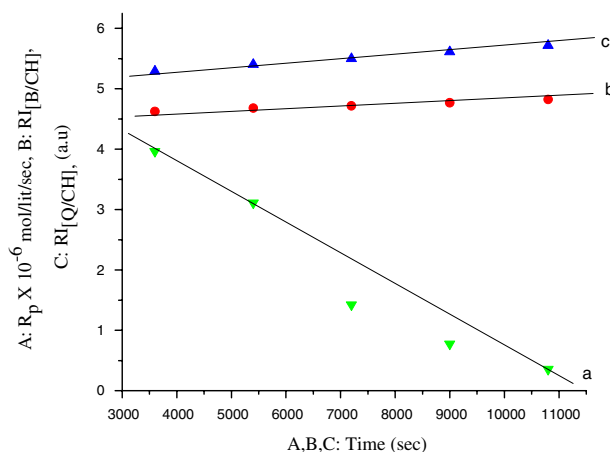


Fig. 3 Effect of time on (a) R_p , (b) $RI_{[B/CH]}$, and (c) $RI_{[Q/CH]}$. [NA] = 0.025 M, [PDS] = 0.025 M, and temperature = $45\text{ }^\circ\text{C}$

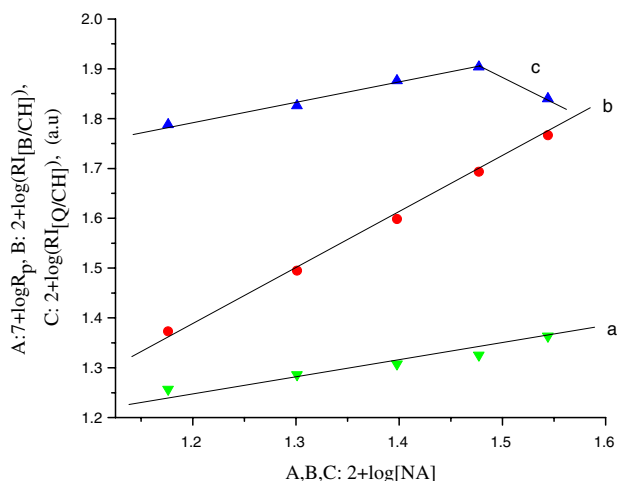


Fig. 4 Effect of [NA] on (a) R_p , (b) $RI_{[B/CH]}$, and (c) $RI_{[Q/CH]}$. [PDS] = 0.025 M, temperature = 45 °C, and time = 2 h

line with a slope value of unity, which indicates the first-order reaction of formation of benzenoid structure with respect to [NA].

We know that benzenoid and quinonoid forms make up PNA backbone. To find out the order of quinonoid ring formation, $\log [NA]$ vs. $\log (RI_{[Q/CH]})$ (Fig. 4c) is made and the slope value is determined as 0.33. This confirmed the 0.50 order of quinonoid structure formation with respect to [NA]. At higher concentration of NA, the RI of [Q/CH] is found to decrease. This is due to the (1) depletion of initiator radicals, (2) doping effect of initiator available rather than available for initiation purpose, and (3) nonavailability of free radicals for polymerization. Quinonoid structure formation may take place in two ways: (1) Primary oxidation of monomer leads to monomer radical cations which on further oxidation (secondary oxidation) lead to the loss of one more electron from amino group of NA monomer. Now the monomer in its secondary oxidation state may couple with another one monomer in its primary or secondary oxidation state and (2) Oxidation of PNA in its leuco-emeraldine state may yield the quinonoid structure. This can be ascribed to the presence of excess of initiator radicals and auto acceleration effect [34], which is caused by PNA chains. Most commonly, the second route is a feasible one because of secondary oxidation of monomer, which leads to the unwanted side products with very high activation energy. Due to lack of literature, our results cannot be compared. For the first time, we report this type of FTIR-based kinetics for conducting polymer nanocomposites.

Effect of [PDS] on R_p and the RI of benzenoid and quinonoid forms of PNA

Figure 5 shows the effect of [PDS] on R_p and RI of amino and imino forms of PNA while other experimental

conditions are kept constant. The R_p value increases continuously with the increase in [PDS]. To find out the order of reaction, the log-log plot is made. The plot of $\log R_p$ vs. $\log [PDS]$ (Fig. 5a) shows a straight line with a slope value of 1.0 and confirms the first-order reaction with respect to [PDS]. This can be explained based on the production of larger amount of initiator radicals $\{R_p \propto [PDS]^{1.0}\}$.

PDS concentration varies between 0.015 and 0.035 M while other experimental conditions are kept constant. When the concentration of PDS is increased, the RI of [B/CH] is increased linearly up to 0.03 M of [PDS] thereafter it shows a decreasing trend due to over oxidation. The order of benzenoid structure formation can be determined by plotting $\log [PDS]$ vs. $\log (RI_{[B/CH]})$ (Fig. 5b) as 1.60. This confirms the 1.50 order of reaction (of benzenoid structure formation) with respect to [PDS]. Under the same experimental conditions, the order of reaction for quinonoid structure formation is determined by plotting $\log [PDS]$ vs. $\log (RI_{[Q/CH]})$ (Fig. 5c) as 0.473. This confirmed the 0.50 order of reaction of quinonoid structure formation with respect to [PDS]. The plot showed a straight line due to the excess availability of free radicals [34] leading to the secondary oxidation of NA or overoxidation of PNA chains.

Effect of temperature on R_p and the RI of benzenoid and quinonoid forms of PNA

At different temperatures, the R_p is calculated while other experimental conditions like [NA], [PDS] and time were kept constant. While increasing the temperature, the R_p value is also increased. This is due to the thermal oxidation of monomeric units and excess availability of heat energy for further initiation process. The energy of activation (E_a) is calculated to be 176.47 kJ/mol from the Arrhenius plot

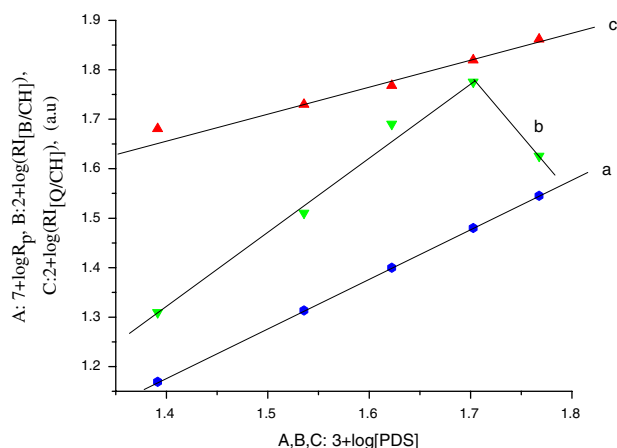


Fig. 5 Effect of [PDS] on (a) R_p , (b) $RI_{[B/CH]}$, and (c) $RI_{[Q/CH]}$. [NA] = 0.025 M, temperature = 45 °C, and time = 2 h

constructed (Fig. 6a). The plot shows the increasing trend of R_p because of higher activation energy.

Change in relative intensity of benzenoid and quinonoid forms of PNA have been tested at different reaction temperature while other experimental conditions are kept constant. Increase in temperature leads to increase in RI of [B/CH] to 55 °C thereafter it shows a drop in RI of [B/CH]. This can be explained as follows: (1) increase in reaction temperature leads to the production of more free radicals from PDS and excess of radicals tutored to secondary oxidation or over oxidation reaction and (2) thermal oxidation of NA radical cations or PNA chains. The energy of activation required for the formation of benzenoid form of PNA can be determined from the Arrhenius plot of $1/T$ vs. $\log(RI_{[B/CH]})$ (Fig. 6b). The E_a value was determined as 181 kJ/mol for benzenoid structure formation in PNA chain. E_a for the quinonoid structure formation in PNA backbone was calculated from the plot of $1/T$ vs. $\log(RI_{[Q/CH]})$ (Fig. 6c) from the slope value as 195 kJ/mol. This indicates that quinonoid form consumes higher amount of heat energy than the benzenoid form.

The E_a values calculated based on R_p and RI have close agreement. Generally, the E_a values are calculated based on R_p , as a bulk system. The E_a values calculated based on RI deal with the trace amount of substance with particular structure formation with polydispersity and resulting with less than 2% error. In this study, the authors attempted to compare the E_a values calculated based on two different methods for the same system and found that these two values have close agreement with each other. Hence, the E_a values calculated based on FTIR-based RI method will be a considerable one.

In the absence of nanomaterial, the order of reaction under different experimental conditions are determined so for. The effect of nanosized materials on the R_p of NA and

the RI of PNA is discussed next. The nanomaterials used here are classified into three categories: (1) metal oxides with the oxidizing nature, doping effect, and surface catalytic effect with layered structure, e.g., V_2O_5 and CrO_3 ; (2) metal oxides having surface catalytic effect with layered structure, e.g., Sb_2O_3 , As_2O_3 , and AHM; and (3) metal oxide acting as a nanofiller with layered structure, e.g., Al_2O_3 , and these are analyzed in the following sections.

Effect of (% weight of V_2O_5) on R_p and the RI of benzenoid and quinonoid forms of PNA

The effect of % weight of V_2O_5 on the R_p of NA is investigated for the first time by our research team. R_p value was determined for different % weight of V_2O_5 while other experimental conditions are kept constant. While increasing the % weight of V_2O_5 from 1 to 9% weight, the R_p value is also increased linearly. To find out the order of dependency, the plot of $\log R_p$ vs. $\log(\% \text{ weight of } V_2O_5)$ (Fig. 7a) is made and the slope value is determined as 1.0 and hence confirms the first-order reaction of (% weight of V_2O_5), i.e., 1 mole of V_2O_5 is required to oxidize 1 mole of NA monomer. This confirms the effective oxidizing nature of V_2O_5 . During the in situ polymerization of NA, V_2O_5 plays a trivial role, i.e., (i) acting as an active oxidizing agent, (ii) accommodate the PNA chain in the interlayer space of V_2O_5 (as a host matrix) with the simultaneous formation of PNA nanocomposite, and (iii) acting as an effective dopant. The conductivity value of PNA is increased by altering the structure of PNA, $\{R_p \propto (\% \text{ Weight of } V_2O_5)^{1.0}\}$. The surface catalytic oxidation behavior of V_2O_5 can be confirmed by analyzing the R_p values. R_p values obtained in the presence of V_2O_5 is greater than that of R_p values in the presence of PDS alone

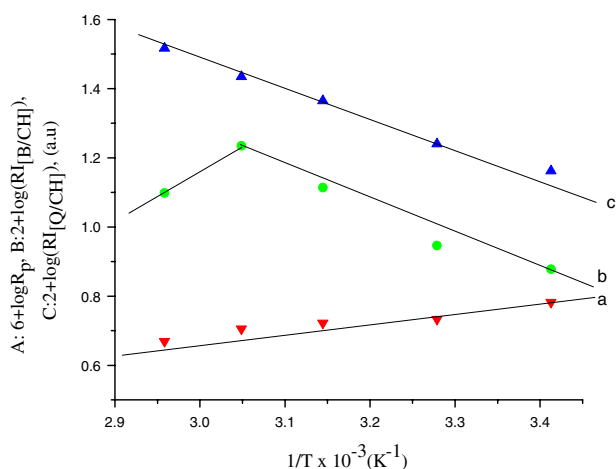


Fig. 6 Effect of temperature on (a) R_p , (b) $RI_{[B/CH]}$, and (c) $RI_{[Q/CH]}$. [NA] = 0.025 M, [PDS] = 0.025 M, and time = 2 h

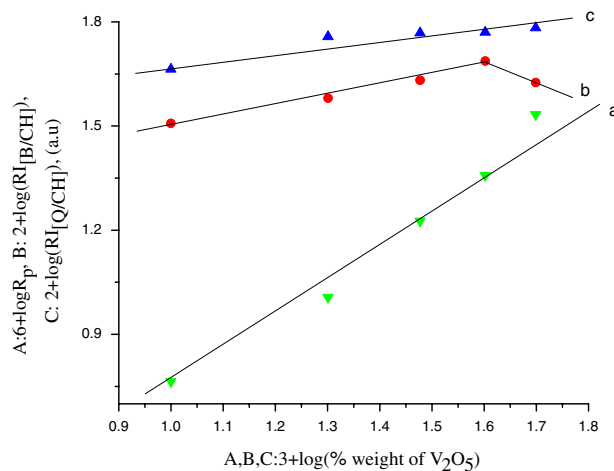


Fig. 7 Effect of (% weight of V_2O_5) on (a) R_p , (b) $RI_{[B/CH]}$, and (c) $RI_{[Q/CH]}$. [NA] = 0.025 M, [PDS] = 0.025 M, temperature = 45 °C, and time = 2 h

(in the absence of V_2O_5). This authenticated the surface catalytic oxidation behavior of V_2O_5 due to the multiple oxidation number of vanadium metal. The host nature of V_2O_5 can be confirmed by seeing the HRTEM images of PNA- V_2O_5 system. The discussion is included separately under HRTEM report. The increase in electrical conductivity of PNA- V_2O_5 nanocomposite system concluded the doping nature of V_2O_5 with PNA matrix. This is the secondary activity of V_2O_5 rather than the primary host nature of V_2O_5 .

V_2O_5 is a well-known oxidizing agent as well as a dopant. Such a versatile nature of chemical agent's role is tested on the chemical structure of PNA/ V_2O_5 nanocomposite. As we know that the chemical structure of PNA is built by both benzenoid and quinonoid structure with different ratio, now, NA is polymerized in the presence of V_2O_5 and its role on the structural prediction is determined. The %weight of V_2O_5 is varied between 1 and 9% while other experimental conditions are kept constant. The increase in %weight of V_2O_5 leads to the increase in the content of both amino and imino forms. The benzenoid form is increased up to 4% weight of V_2O_5 thereafter it shows a decreasing trend because of over oxidation due to surface effect of V_2O_5 on PNA structure. To find out the order of reaction, the following plot is made between \log (% weight of V_2O_5) and \log ($RI_{[B/CH]}$) (Fig. 7b). The plot showed a straight line with the slope value of 0.27 and followed the 0.25 order of formation of benzenoid structure with respect to % weight of V_2O_5 . This explains the efficiency of V_2O_5 toward the building of structure of PNA particularly with the benzenoid structure formation. Moreover, V_2O_5 plays the trivial role in the in situ polymerization of NA. Similarly, the role of V_2O_5 on the quinonoid structure formation was tested under identical experimental conditions. While increasing the % weight of V_2O_5 , the quinonoid forms are also increased linearly. This is due to the over oxidation of benzenoid structure. From the plot of \log (% weight of V_2O_5) vs. \log ($RI_{[Q/CH]}$) (Fig. 7c), the slope value is determined as 0.21 which confirms the 0.25 order of reaction of quinonoid structure formation with respect to % weight of V_2O_5 . This clearly explains that during the in situ polymerization process, the PNA chains are intercalated into the basal spacing of V_2O_5 and hence acts as a host matrix. In addition, due to its surface catalytic effect, V_2O_5 activates the formation of PNA structure with the increase of electrical conductivity value. This proves the doping nature of V_2O_5 . Hence, the trivial role of V_2O_5 is proved through the formation of PNA- V_2O_5 nanocomposite. Our previous publication on PDS-initiated polymerization of NA in the presence of nanosized clay infers that the added clay accelerated the formation of benzenoid structure rather than the quinonoid structure [34]. By comparing these results, we can arrive at

a conclusion that acceleration of benzenoid or quinonoid form of PNA depends on the nature and size of nanomaterials which is used for making polymer nanocomposite.

Effect of (% weight of CrO_3) on R_p and the RI of benzenoid and quinonoid forms of PNA

Effect of % weight of CrO_3 on the structure of PNA was tested between 1 and 9 % weight of CrO_3 . It is interesting to note that while increasing the % weight of CrO_3 , the R_p is also increased. The increase in R_p can be accounted by the following reasons. First, strong oxidizing nature of CrO_3 ; second, complex formation of Cr^{6+} ion with the NA monomer-PDS initiator; third, insertion of NA monomer or PNA units inside the basal spacing of CrO_3 ; and finally, surface catalytic effect of CrO_3 . Generally, the multivalent metal ions have complex forming capability. When NA is mixed with CrO_3 , there will be a formation of complex between NA and CrO_3 . In such a way it attracts NA monomeric units until it forms Cr^{3+} , then oxidizes (attraction or insertion and oxidation should be a simultaneous process) the monomeric units and results in the intercalation of PNA chains into the basal spacing of CrO_3 . Discussion on intercalation of PNA into CrO_3 is separately provided under HRTEM report. To find out the order of reaction, the plot of $\log R_p$ vs. \log (% weight of CrO_3) is drawn and shown in Fig. 8a. The plot shows a straight line with the slope value of 0.10 and confirms the 0.10 order dependence of R_p with respect to the % weight of CrO_3 ($R_p \propto (\% \text{ weight of } CrO_3)^{0.10}$).

Polymer nanocomposite synthesized under the same experimental conditions were subjected to the measurement of RI corresponding to amino(benzenoid) and imino(quinonoid) forms of PNA. While increasing the % weight of CrO_3 , the benzenoid structure is increased initially and then it follows the decreasing trend. This explains the strong oxidizing nature of CrO_3 in the reaction medium. Determination of slope value of the plot of \log (% weight of CrO_3) vs. \log ($RI_{[B/CH]}$) explains the order of reaction. The slope value is determined from Fig. 8b in the linear region as 0.56. This confirms the 0.50 order of reaction of benzenoid structure formation with respect to % weight of CrO_3 . Figure 8c explains the plot of \log (% weight of CrO_3) vs. \log ($RI_{[Q/CH]}$) that indicates the straight line with the slope value of 0.21. The straight line indicates the strong oxidizing nature of CrO_3 on the polymerization particularly of quinonoid structure formation. This proves the 0.25 order of formation of quinonoid structure with respect to % weight of CrO_3 . Furthermore, it can be explained by providing space for the guest PNA chains and in such a way interacting with PNA chains as a dopant as well as a host matrix.

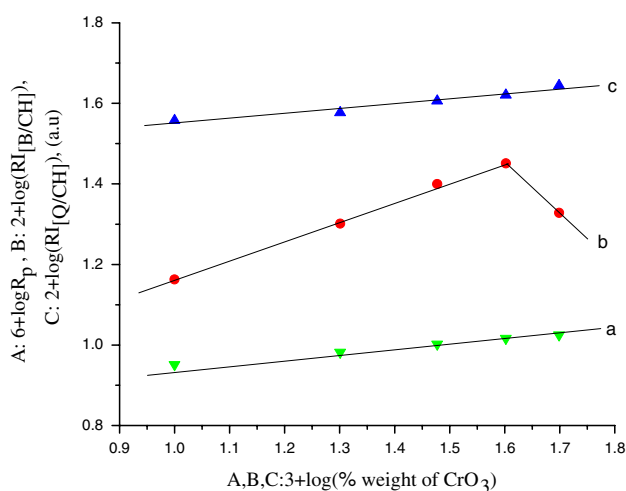


Fig. 8 Effect of (% weight of CrO_3) on (a) R_p , (b) $\text{RI}_{[\text{B/CH}]}$, and (c) $\text{RI}_{[\text{Q/CH}]}$. $[\text{NA}] = 0.025 \text{ M}$, $[\text{PDS}] = 0.025 \text{ M}$, temperature = 45°C , and time = 2 h

Effect of (% weight of Sb_2O_3) on R_p and the RI of benzenoid and quinonoid forms of PNA

The next category of nanomaterials is the host matrix with layered structure. These materials do not have oxidizing capability. They can simply provide a space for the accommodation of guest molecules without any interaction with the guest and in such a way, they can form nanocomposite with PNA. However, due to their high surface area, they can accelerate the polymerization reaction by adsorption mechanism. As usual, the % weight of Sb_2O_3 varied between 1 and 9. The variation in % weight reflects on the R_p value. To study the order of reaction, the plot of $\log(\% \text{ weight of } \text{Sb}_2\text{O}_3)$ vs. $\log R_p$ (Fig. 9a) was drawn and the slope value is noted as 2.0. It means that two molecules of Sb_2O_3 are required to accelerate one mole of NA monomeric unit. Hence, R_p follows the second-order reaction with respect to % weight of Sb_2O_3 . This value is entirely different from the other nanomaterials used for the preparation of polymer nanocomposites. This explains the host–guest mechanism. The order of reaction indirectly explains the agglomeration nature of nanomaterial during the in situ polymerization with NA $\{R_p \propto (\% \text{ weight of } \text{Sb}_2\text{O}_3)^{2.0}\}$.

The role of Sb_2O_3 on the benzenoid and quinonoid structure of PNA was tested with samples synthesized under the same experimental conditions. At lower % weight of Sb_2O_3 , the benzenoid structure formation is activated, whereas at higher % weight of Sb_2O_3 , due to agglomeration process, the benzenoid structure content is reduced. The plot also explains the same truth. The plot of $\log(\% \text{ weight of } \text{Sb}_2\text{O}_3)$ vs. $\log(\text{RI}_{[\text{B/CH}]})$ (Fig. 9b) gives a slope value of 0.56, which confirms the 0.50 order of

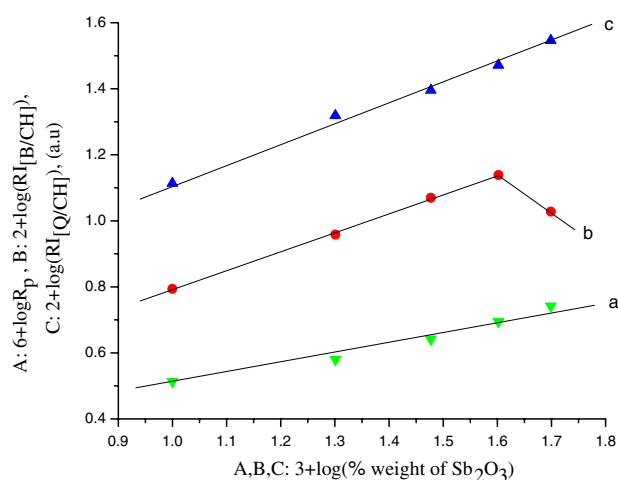


Fig. 9 Effect of (% weight of Sb_2O_3) on (a) R_p , (b) $\text{RI}_{[\text{B/CH}]}$, and (c) $\text{RI}_{[\text{Q/CH}]}$. $[\text{NA}] = 0.025 \text{ M}$, $[\text{PDS}] = 0.025 \text{ M}$, temperature = 45°C , and time = 2 h

reaction of benzenoid structure formation with respect to % weight of Sb_2O_3 . Similarly, the effect of Sb_2O_3 on the quinonoid structure formation was also tested. Here, one can find a straight line with the increase of % weight of Sb_2O_3 . Due to agglomeration nature of Sb_2O_3 at higher % weight, the primarily oxidized NA radical cations are further subjected to secondary oxidation reaction. In addition, there is chance for the further oxidation of leucoemeraldine-type PNA to emeraldine salt-like structure. $\log(\% \text{ weight of } \text{Sb}_2\text{O}_3)$ vs. $\log(\text{RI}_{[\text{Q/CH}]})$ (Fig. 9c) plot generates a straight line with the slope value of 0.58, which, again, confirms the 0.50 order of reaction of quinonoid structure formation with respect to % weight of Sb_2O_3 .

Effect of (% weight of As_2O_3) on R_p and the RI of benzenoid and quinonoid forms of PNA

We study the effect of host matrix on the structure–property relationship of PNA. The next host matrix with layered structure is As_2O_3 . The % weight of As_2O_3 is varied between 1 and 9 while other experimental conditions were kept constant under nitrogen atmosphere at 45°C . The R_p value is linearly increasing with the increase of % weight of As_2O_3 . Figure 10a represents the plot of $\log(\% \text{ weight of } \text{As}_2\text{O}_3)$ vs. $\log R_p$ with a straight line. To find out the order of reaction, the slope value is essential. The same can be determined from the Fig. 10a as 0.23. This confirms the 0.25 order of reaction with respect to % weight of As_2O_3 . The increase in R_p is due to the host matrix and catalytic activity due to the high surface area of As_2O_3 $\{R_p \propto (\% \text{ weight of } \text{As}_2\text{O}_3)^{0.23}\}$.

The FTIR study informs the structure of benzenoid and quinonoid forms of PNA. By using the relative intensity values, again we apply the chemical kinetics to find out the

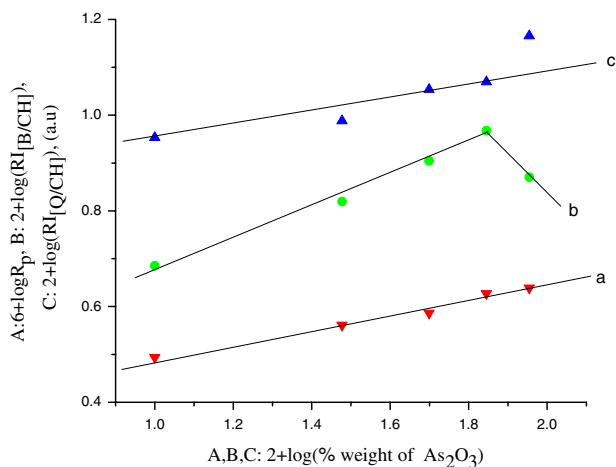


Fig. 10 Effect of (% weight of As_2O_3) on (a) R_p , (b) $\text{RI}_{[\text{B}/\text{CH}]}$, and (c) $\text{RI}_{[\text{Q}/\text{CH}]}$. $[\text{NA}] = 0.025 \text{ M}$, $[\text{PDS}] = 0.025 \text{ M}$, temperature = 45°C , and time = 2 h

content of amino and imino forms of PNA rather than the chemical analysis method. The order of benzenoid and quinonoid structure formation can be determined from the plots of $\log(\% \text{ weight of } \text{As}_2\text{O}_3)$ vs. $\log(\text{RI}_{[\text{Q}/\text{CH}]})$ (Fig. 10b) and $\log(\% \text{ weight of } \text{As}_2\text{O}_3)$ vs. $\log(\text{RI}_{[\text{Q}/\text{CH}]})$ (Fig. 10c), respectively, and the slope values are as follows: 0.52 and 0.35. These two values confirm that both benzenoid and quinonoid forms of PNA follow the 0.50 order of reaction with respect to $\% \text{ weight of } \text{As}_2\text{O}_3$. This is due to the simple catalytic effect and host matrix nature of As_2O_3 .

Effect of (% weight of AHM) on R_p and the RI of benzenoid and quinonoid forms of PNA

The last material with layered structure is nano AHM. Effect of (% weight of AHM) on R_p is tested while other experimental conditions are kept constant. To find out the order of reaction, the following log-log plot (Fig. 11a) is drawn and the plot shows the increasing trend with the slope value of 0.59. This infers that the R_p is 0.50 order of reaction with respect to (% weight of AHM). The increase in R_p of NA can be explained on the basis of surface catalytic activity of AHM and the intercalation of PNA chains into the inter layer space of AHM $\{R_p \propto (\% \text{ weight of AHM})^{0.50}\}$.

The host AHM plays considerable role in the structure building process. During the in situ polymerization process, intercalation of PNA chains into the interlayer space of AHM is a typical reaction. In which the polymer chains are not oxidized further, instead the PNA chains present outside the basal spacing is exposed to further interaction with radicals. As a result, there will be formation of more quinonoid structure activation at higher % weight of AHM.

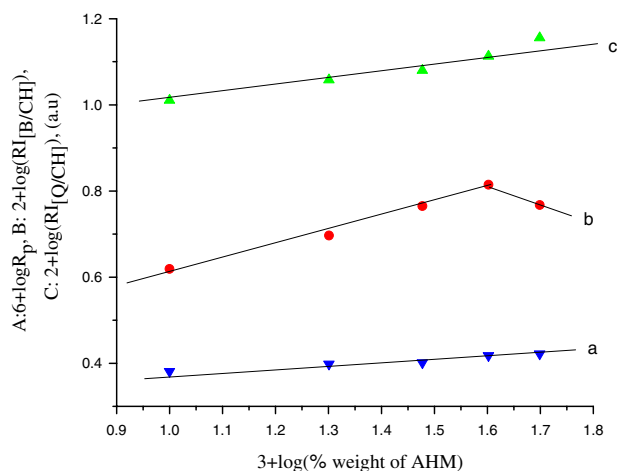


Fig. 11 Effect of (% weight of AHM) on (a) R_p , (b) $\text{RI}_{[\text{B}/\text{CH}]}$, and (c) $\text{RI}_{[\text{Q}/\text{CH}]}$. $[\text{NA}] = 0.025 \text{ M}$, $[\text{PDS}] = 0.025 \text{ M}$, temperature = 45°C , and time = 2 h

The temperature, driving force, also facilitates the above-mentioned reaction. Hence, the quinonoid structure formation shows linearity with respect to % weight of AHM. Figure 11b and c shows the plots of $\log(\% \text{ weight of AHM})$ vs. $\log(\text{RI}_{[\text{B}/\text{CH}]})$ and $\log(\% \text{ weight of AHM})$ vs. $\log(\text{RI}_{[\text{Q}/\text{CH}]})$, respectively, with slope value of 0.33 and 0.35 correspondingly. These values confirm the 0.50 order of reaction for both benzenoid and quinonoid structure formation with respect to % weight of AHM.

Effect of (% weight of Al_2O_3) on R_p and the RI of benzenoid and quinonoid forms of PNA

The last nanomaterial with filler-like behavior is Al_2O_3 . The added alumina has a layered brucite-like structure; it simply occupies the empty space between the PNA chains as a filler. During the filling process, there is no chemical interaction between the alumina and PNA chains. Due to the presence of such a heterogeneous material, the structure and property of PNA is altered. The R_p values and RI of both benzenoid and quinonoid forms are altered by the alumina. Figure 12a shows the plot of $\log(\% \text{ weight of } \text{Al}_2\text{O}_3)$ vs. $\log R_p$ with a straight line, and the slope value is calculated as 0.28, which confirms the 0.25 order of reaction with respect to % weight of Al_2O_3 $\{R_p \propto (\% \text{ weight of } \text{Al}_2\text{O}_3)^{0.28}\}$.

Similarly, the structure of PNA was also affected by the effect of Al_2O_3 . The content of benzenoid structure is increased to 7% weight of Al_2O_3 , whereas at higher % weight of Al_2O_3 , it reduced the formation of benzenoid structure. This is associated with the agglomeration process and resulted in bundle-like structure. The plot of $\log(\% \text{ weight of } \text{Al}_2\text{O}_3)$ vs. $\log(\text{RI}_{[\text{B}/\text{CH}]})$ (Fig. 12b) and $\log(\% \text{ weight of } \text{Al}_2\text{O}_3)$ vs. $\log(\text{RI}_{[\text{Q}/\text{CH}]})$ (Fig. 12c) was drawn,

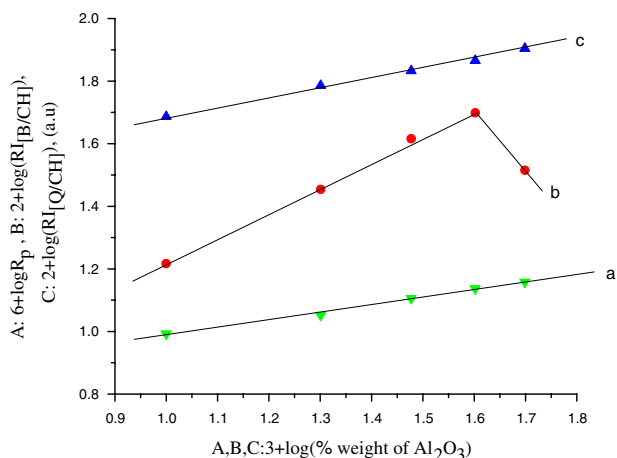


Fig. 12 Effect of (% weight of Al_2O_3) on (a) R_p , (b) $\text{RI}_{[\text{B}/\text{CH}]}$, and (c) $\text{RI}_{[\text{Q}/\text{CH}]}$. $[\text{NA}] = 0.025 \text{ M}$, $[\text{PDS}] = 0.025 \text{ M}$, temperature = $45 \text{ }^\circ\text{C}$, and time = 2 h

and the slope values were determined as 0.80 and 0.30, respectively, for benzenoid and quinonoid structure formation with respect to % weight of Al_2O_3 . Generally, the brucite-like layer structure holds carbonate anion in its interlayer space and exchange of anion with the present system is not possible and hence alumina is simply acting as a filler.

TGA profiles

The thermal stability of PNA and its nanocomposites are represented in Fig. 13 and Table 1. Thermogram of PNA (Fig. 13a) shows a two-step degradation process. The first minor weight loss before $200 \text{ }^\circ\text{C}$ is due to the removal of moisture, water, and dopants, whereas the second major weight loss step around $500 \text{ }^\circ\text{C}$ is associated with the degradation of PNA backbone. Below $650 \text{ }^\circ\text{C}$, all the PNA are decomposed completely. In the case of PNA nanocomposites, the thermal stability is increased. Figure 13b represents the thermogram of $\text{PNA-V}_2\text{O}_5$ nanocomposite. At $400 \text{ }^\circ\text{C}$, it shows the weight of 88%. The % weight residue remains above $700 \text{ }^\circ\text{C}$, which is 53.5%. TGA of PNA-AHM is shown in Fig. 13c. Here also one can see the increment in thermal stability. At $400 \text{ }^\circ\text{C}$ and above $750 \text{ }^\circ\text{C}$, it shows 75% and 44.5% weight, respectively, whereas As_2O_3 shows the 86% and 43.8% weight, respectively (Fig. 13d). For PNA-CrO_3 (Fig. 13e), Al_2O_3 (Fig. 13f), and Sb_2O_3 (Fig. 13g) systems, the following is the % weight at $400 \text{ }^\circ\text{C}$ and above $750 \text{ }^\circ\text{C}$: 82, 85, and 84% and 22, 45, and 31% weight, respectively (Table 1). The above data infers that while making PNA nanocomposite, the thermal stability of PNA is highly increased. The increase in thermal stability is due to the following reasons: (1) metal oxides have layered structure in which, the NA

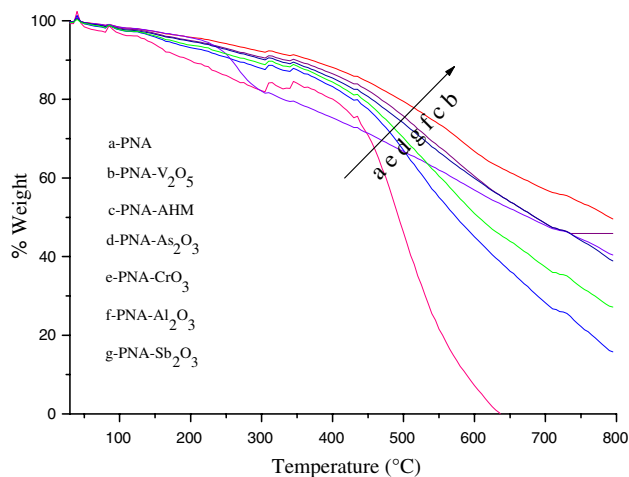


Fig. 13 TGA of (a) PNA, (b) $\text{PNA-V}_2\text{O}_5$, (c) PNA-AHM , (d) $\text{PNA-As}_2\text{O}_3$, (e) PNA-CrO_3 , (f) $\text{PNA-Al}_2\text{O}_3$, and (g) $\text{PNA-Sb}_2\text{O}_3$. $[\text{NA}] = 0.025 \text{ M}$, $[\text{PDS}] = 0.025 \text{ M}$, time = 2 h, temperature = $45 \text{ }^\circ\text{C}$, and nanomaterial = 5% weight

Table 1 TGA data of PNA and its nanocomposites

System	% Weight at $200 \text{ }^\circ\text{C}$	% Weight at $400 \text{ }^\circ\text{C}$	% Weight at $600 \text{ }^\circ\text{C}$	% Weight above $750 \text{ }^\circ\text{C}$
PNA	89.96	79.73	6.79	–
PNA-AHM	94.70	75.18	56.82	44.50
$\text{PNA-V}_2\text{O}_5$	95.71	88.02	66.86	53.54
$\text{PNA-As}_2\text{O}_3$	94.70	86.35	60.36	43.86
PNA-CrO_3	93.03	82.84	45.56	22.33
$\text{PNA-Al}_2\text{O}_3$	94.91	85.34	59.49	45.45
$\text{PNA-Sb}_2\text{O}_3$	93.98	84.45	51.66	31.95

radical cations are intercalated, (2) existence of secondary forces like hydrogen bonding, dipole–dipole interaction between metal oxide, and PNA, (3) metal oxides are acting as an effective dopant, and (4) sometimes the metal oxides can create charges on the surface of PNA. During the in situ polymerization of NA in the presence of metal oxide, there is a chance for the intercalation of NA radical cations into the layered structure (basal spacing) of metal oxides, or the platelets of metal oxides can be exfoliated and dispersed uniformly on the polymer matrix with secondary forces. This accounted for the increase in thermal stability of PNA. Recently, Anbarasan et al. [36] explained the intercalation of PANI into the basal spacing of clay and increased thermal stability of PANI. The added clay protects the PANI chain from thermal forces (through umbrella process) and increases the char forming behavior at higher temperature. Ma et al. [37] synthesized PANI/ HTiNbO_5 lamellar hybrid nanocomposite and characterized by using FTIR, SEM, TGA, and cyclic voltammetry techniques. Our TGA results are in agreement with the above-mentioned study [37].

AFM reports

AFM photographs of polymer and polymer nanocomposites are shown in Figs. 14, 15, 16, 17, 18, 19, and 20. The cage-like structure of pristine PNA is shown in

Fig. 14. Whereas the AFM image of other PNA nanocomposite shows the distorted spherical morphology with the particle size of approximately 35 nm. Hence, AFM confirmed the presence of nanomaterials in the PNA nanocomposites.

Fig. 14 AFM of PNA.

[NA] = 0.025 M,
[PDS] = 0.025 M, time = 2 h,
temperature = 45 °C, and
nanomaterial = 5% weight

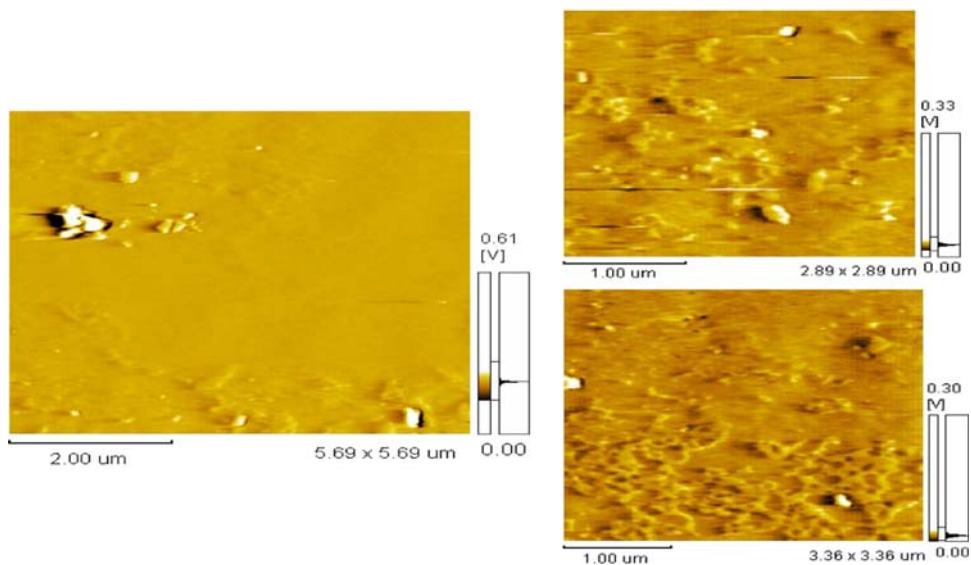


Fig. 15 (a) AFM and (b) HRTEM images of PNA–5% weight V_2O_5 system.

[NA] = 0.025 M,
[PDS] = 0.025 M, time = 2 h,
temperature = 45 °C, and
nanomaterial = 5% weight

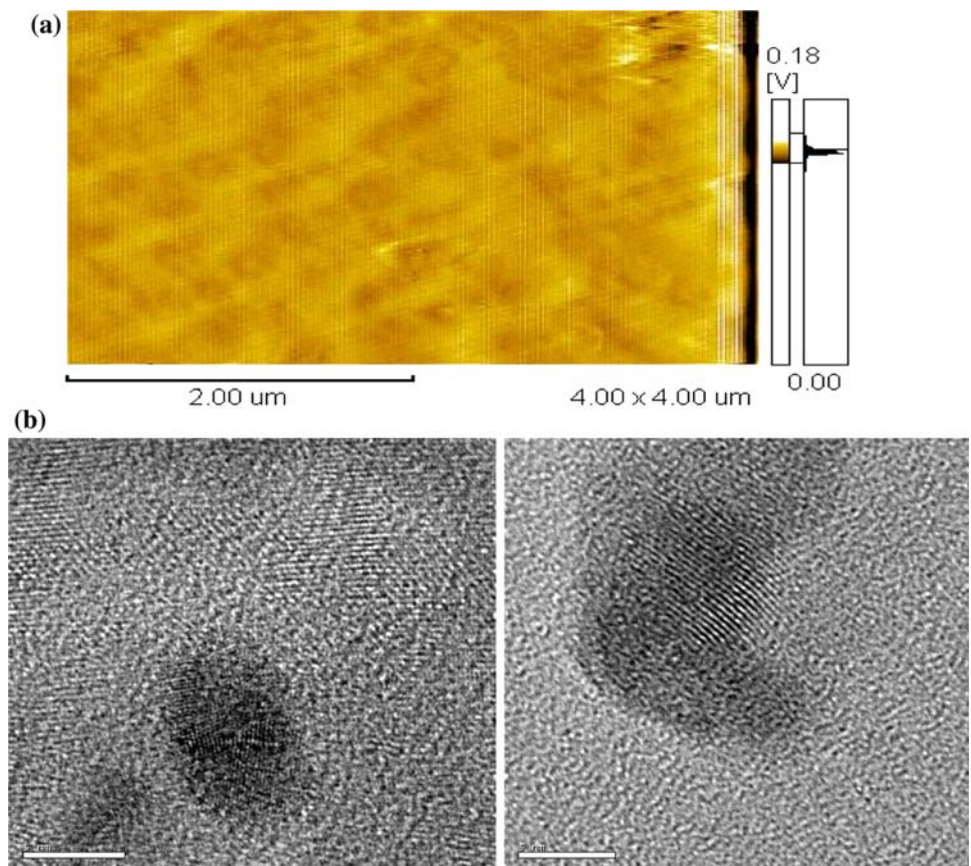
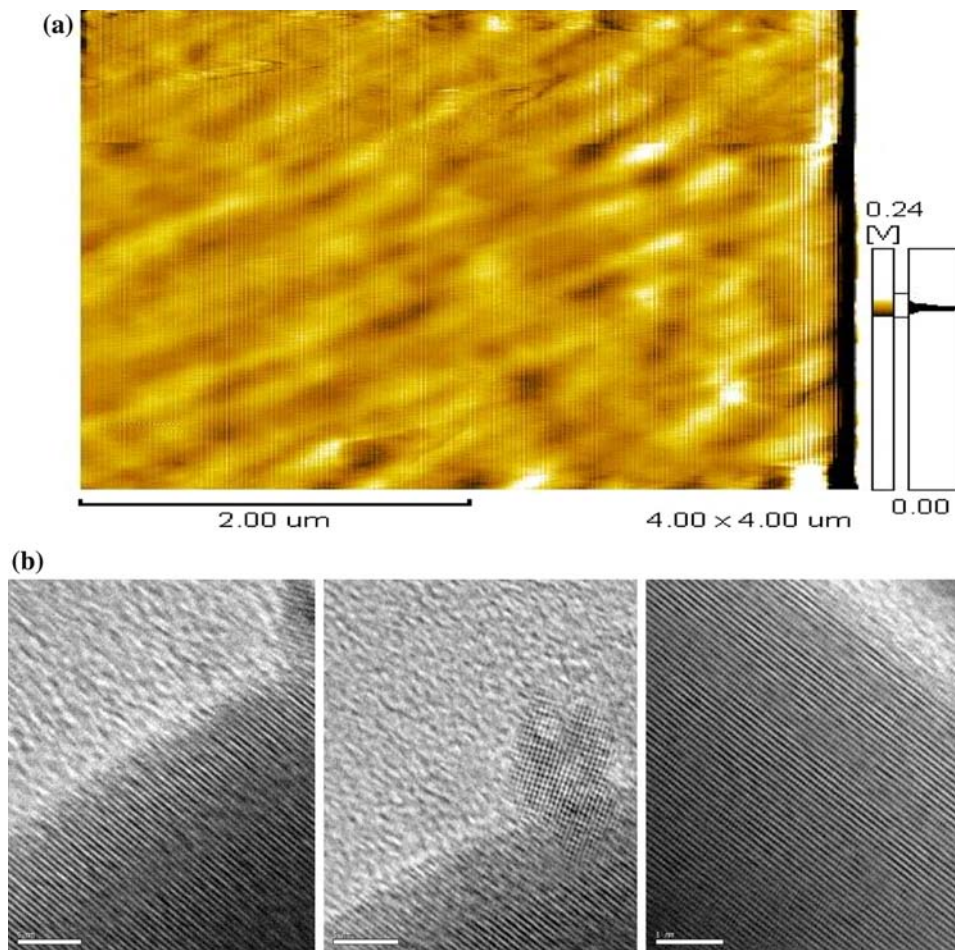


Fig. 16 (a) AFM and (b) HRTEM topography of PNA–5% weight CrO_3 system. [NA] = 0.025 M, [PDS] = 0.025 M, time = 2 h, temperature = 45 °C, and nanomaterial = 5% weight



HRTEM reports

Figure 15b represent the HRTEM images of PNA– V_2O_5 (5% weight) nanocomposite system. The layered structure of V_2O_5 (with the size of 10–15 nm) is intercalated with PNA chains. This can be seen as black dots in between the layered structure of V_2O_5 . This concluded that during the in situ polymerization of NA, intercalation of PNA chains into the basal spacing of V_2O_5 occurred simultaneously. Figure 16b indicate the HRTEM topography of PNA intercalated CrO_3 (5% weight) system. The layered structure of CrO_3 with the size of 25–30 nm was accommodated with PNA chains in its basal spacing. Due to intercalation reaction, the layered structure of CrO_3 was broken with the dark spots. This confirmed the interaction between PNA chains and CrO_3 nanosystem.

Conductivity

The conductivity value of parent PNA is determined as 4.81×10^{-3} S/cm. On the addition of 0.05 g of CrO_3 , the conductivity value is raised to 1.37×10^{-2} S/cm.

Similarly, while adding 0.05 g of Sb_2O_3 , V_2O_5 , As_2O_3 , Al_2O_3 , and AHM, the conductivity values are 6.89×10^{-2} , 8.42×10^{-2} , 5.17×10^{-3} , 5.64×10^{-3} , and 12.89×10^{-3} S/cm, respectively. The increase in conductivity may be due to the formation of charge on the PNA surface. The metal oxides through their secondary forces of attraction can create the charge on the surface of PNA. This is in accordance with our earlier publication [36]. While increasing the % weight of nanomaterial, the electrical conductivity value of PNA is slightly increased.

Conclusions

By using the chemical solution polymerization method, we have successfully synthesized PNA and its nanocomposites. FTIR spectroscopy provides the characteristic stretching vibrations of amino(benzenoid form) and imino(quinoid form) forms of PNA. Presence of nanosized materials can be identified in the finger print region particularly from 400 to 1000 cm^{-1} . The kinetic results inferred that the first-order dependence with initiator concentration and 1.75-order dependence with monomer

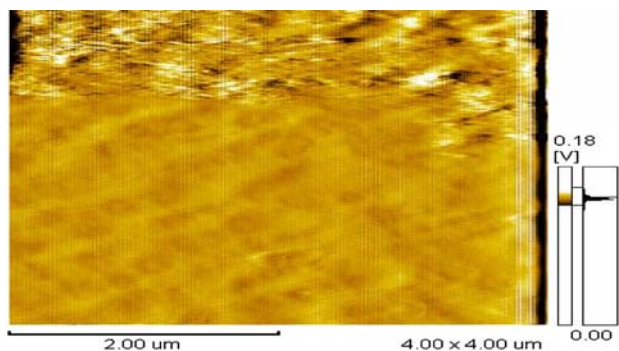


Fig. 17 AFM of PNA–5% weight of Sb_2O_3 . [NA] = 0.025 M, [PDS] = 0.025 M, time = 2 h, temperature = 45 °C, and nanomaterial = 5% weight

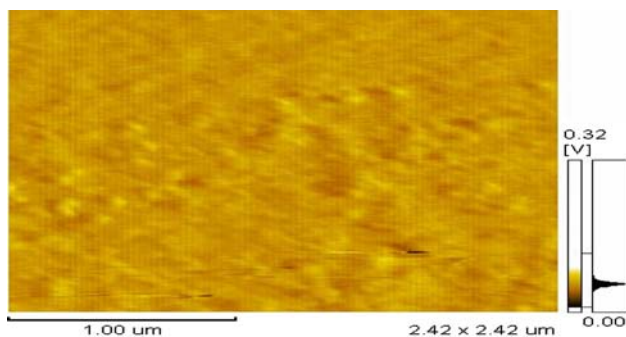


Fig. 18 AFM of PNA–5% weight of As_2O_3 . [NA] = 0.025 M, [PDS] = 0.025 M, time = 2 h, temperature = 45 °C, and nanomaterial = 5% weight

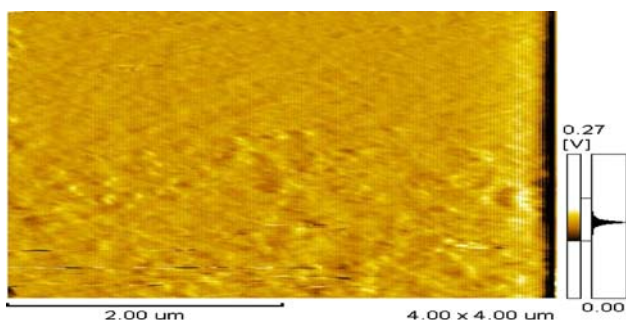


Fig. 19 AFM of PNA–5% weight of Al_2O_3 . [NA] = 0.025 M, [PDS] = 0.025 M, time = 2 h, temperature = 45 °C, and nanomaterial = 5% weight

concentration. While changing the (% weight of nanomaterials), the R_p value is also changed because of its surface catalytic effect, due to larger surface area of nanosized quasi-one-dimensional metal oxides. TGA confirms the increase in char forming capability of PNA in the presence of nanosized materials. The % weight residue remains above 700 °C is drastically increased with the increase of % weight of nanomaterials. The added nanosized materials also accelerate the conductivity value of the PNA. AFM

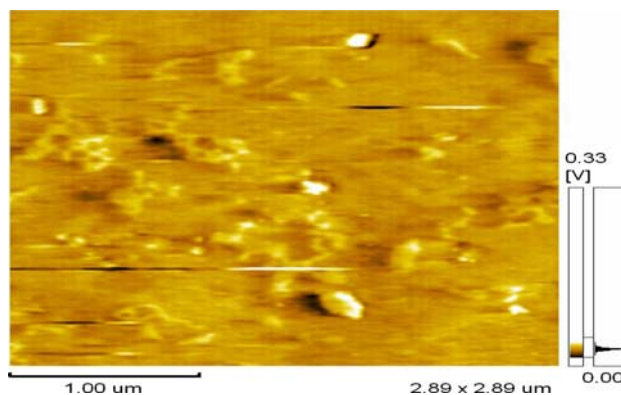


Fig. 20 AFM of PNA–5% weight of AHM. [NA] = 0.025 M, [PDS] = 0.025 M, time = 2 h, temperature = 45 °C, and nanomaterial = 5% weight

confirms the presence of approximately 25- to 40-nm-sized metal oxide particles in the PNA nanocomposites. HRTEM confirmed the intercalation of PNA chains into the basal spacing of metal oxides.

References

- Eftekhari A, Afshani R (2006) J Polym Sci A: Polym Chem 44:3304. doi:10.1002/pola.21422
- Fonseca M, Rinaldi A, Rubira AF, Cotica LF (2006) Mater Chem Phys 97:252. doi:10.1016/j.matchemphys.2005.08.007
- Gupta N, Sharma S, Mir IA (2006) J Sci Ind Res 65:549
- Baghahi SM, Beigi AM, Legheri A, Teymouri M (2002) Iran Polym J 11:387
- Entazami A, Golabi SM, Raof J (1992) Iran J Polym Sci Technol 1:7
- Genies EM, Lapkowski M (1987) Electrochim Acta 32:1223
- Li X, Sun C, Wei Z (2005) Synth Met 155:45. doi:10.1016/j.synthmet.2005.05.020
- Moon DK, Osakada K, Kubota K (1993) Macromolecules 26:6992. doi:10.1021/ma00077a042
- Schmitz BK, Euler WB (1995) J Electronal Chem 399:47
- Arevalo AH, Fernandez H, Silber JJ, Sereno L (1990) Electrochim Acta 35:741
- Xu X, Xie O, Hu M, Nie L, Yao S (1995) J Electroanal Chem 389:85
- Roy BC, Gupta MD, Bowmick L, Ray JK (2003) Bull Mater Sci 26:633
- George V, Young DY (2002) Polymer 43:4073
- Gordana CM, Cvjeticani N, Simendic JB, Krakovsky I (2003) Polym Bull 50:319. doi:10.1007/s00289-003-0174-8
- Faria R, Bulhoes L (1998) Electrochim Acta 44:95
- Huang SS, Li J, Lin HG, Yu RO (1995) Mikrochim Acta 117:145
- Gordana CM, Marjanovic B, Antic V, Juramic I (2002) J Serb Chem Soc 67:867
- Omrani A, Simon LC, Rostami AA, Ghaemy M (2008) Int J Chem Kinet 40:663. doi:10.1002/kin.20350
- Svegl F, Orel B (2003) Mater Technol 37:29
- Copikova J, Synytsya A, Novotna M (2001) Czech J Food Sci 19:51
- Wang JS, Shi JS, Wu JG (2003) World J Gastroenterol 9:1897
- Xueref I, Domine F (2003) Atmos Chem Phys 3:1779

23. Matkovic SM, Valle GM, Briand LE (2005) *Latin Am Appl Phys* 35:189
24. Schwendtner K, Libowitzky E, Koss S (2003) *Geophys Res Abstr* 5:06826
25. Asimow PD, Stein LC, Rinsman GR (2006) *Am Mineral* 91:278. doi:[10.2138/am2006.1937](https://doi.org/10.2138/am2006.1937)
26. van de Voort FR, Sedman J, Mucciardi C (2004) *Appl Spectrosc* 58:193
27. Parker JR, Waddell WH (1996) *J Elast Plast* 28:140
28. Saule M, Navarre S, Babout O, Maillard B (2003) *Macromolecules* 36:7469. doi:[10.1021/ma0342325](https://doi.org/10.1021/ma0342325)
29. Saule M, Navarre S, Babout O, Maillard B (2005) *Macromolecules* 38:77. doi:[10.1021/ma048712n](https://doi.org/10.1021/ma048712n)
30. Navarre S, Maillard B (2000) *J Polym Sci Part A Chem Ed* 38:2957. doi:[10.1099-0518-\(20000815\)38:16<2957](https://doi.org/10.1099-0518-(20000815)38:16<2957)
31. Anbarasan R, Babout O, Dequiel M, Maillard B (2005) *J Appl Polym Sci* 97:761. doi:[10.1002/app.21342](https://doi.org/10.1002/app.21342)
32. Anbarasan R, Babout O, Dequiel M, Maillard B (2005) *J Appl Polym Sci* 97:766. doi:[10.1002/app.21343](https://doi.org/10.1002/app.21343)
33. Duraimurugan K, Rathiga S, Baskaran I, Anbarasan R (2008) *Chin J Polym Sci* 26:393. doi:[10.1142/s0256767908003059](https://doi.org/10.1142/s0256767908003059)
34. Anbarasan R, Anandhakrishnan R, Vivek G (2008) *Polym Compos* 29:949. doi:[10.1002/pc.20462](https://doi.org/10.1002/pc.20462)
35. Chang Q, Zhao K, Chen X, Li M, Liu J (2008) *J Mater Sci* 43:5861. doi:[10.1007/s10853-008-2827-3](https://doi.org/10.1007/s10853-008-2827-3)
36. Anbarasan R, Sivakumaravel S, Gopiganesh G (2006) *Int J Polym Mater* 55:803
37. Ma J, Zhang X, Yan C, Tong Z, Inoue H (2008) *J Mater Sci* 43:5534. doi:[10.1007/s10853-008-2837-1](https://doi.org/10.1007/s10853-008-2837-1)